Negative thermal expansion and local dynamics in Cu_2O and Ag_2O

A. Sanson and F. Rocca
IFN, Istituto di Fotonica e Nanotecnologie del Consiglio Nazionale delle Ricerche, Sezione CeFSA di Trento-38050 Povo (Trento), Italy

G. Dalba, P. Fornasini,* and R. Grisenti
Istituto Nazionale per la Fisica della Materia and Dipartimento di Fisica, Università di Trento, Via Sommarive 14, I-38050 Povo (Trento), Italy

M. Dapiaggi and G. Artioli
Dipartimento di Scienze della Terra "Ardito Desio," Università di Milano, via Botticelli 23, I-20133 Milano, Italy
(Received 8 March 2006; published 20 June 2006)

High-resolution x-ray powder diffraction and extended x-ray-absorption fine-structure (EXAFS) measurements have been performed on the iso-structural framework crystals Cu_2O and Ag_2O as a function of temperature. According to diffraction, both compounds exhibit a negative thermal expansion (NTE) of the lattice parameter over extended temperature intervals (from 9 to 240 K for Cu_2O, up to 470 K for Ag_2O) and anisotropic thermal displacements of M atoms (M=Cu,Ag). EXAFS measures a positive expansion of the nearest-neighbors M-O pair distance and a perpendicular to parallel anisotropy of relative motion, much stronger than the anisotropy of the absolute M motion. The M-O bond is much stiffer against stretching than against bending. According to EXAFS, out of the 12 M-M next-nearest-neighbor pairs, the 6 connected via a bridging oxygen undergo negative expansion, while the 6 lacking the bridging oxygen undergo positive expansion. These results show a rather complex local behavior, which, while confirming the connection of NTE to strong perpendicular vibrations, is inconsistent with rigid unit modes models and suggests a more flexible model based on rigid M-O rods.

DOI: 10.1103/PhysRevB.73.214305 PACS number(s): 65.40.De, 63.20.Ry, 87.64.Fb

I. INTRODUCTION

Negative thermal expansion (NTE) can affect, in limited temperature intervals, simple crystals with tetrahedral coordination, like silicon or GaAs.[1–3] This effect has been attributed to low-frequency transverse modes with negative Grüneisen parameter.[4] Recently, the interest toward NTE has been renewed by the discovery of crystals exhibiting strong NTE over large temperature intervals, like ZrW_2O_8 (NTE from 0.3 to 1050 K),[5] Ag_2O (NTE from 10 to 500 K),[6] $Zn(CN)_2$ (NTE from 100 to 400 K).[7] Systems with zero thermal expansion (ZTE) have also been found.[8,9] NTE and ZTE materials are technologically interesting for the production of composites with specifically tailored thermal expansivities.[10]

Many crystals affected by NTE over large temperature intervals, like ZrW_2O_8 or Ag_2O, exhibit framework structures, which are often depicted as formed by corner-sharing polyhedral structural units. The macroscopic thermal expansion in framework structures is generally considered the result of a competition between a positive contribution due to bond stretching and a negative contribution of geometrical origin, often attributed to low-frequency rigid unit modes (RUMs),[11] which cause rigid rotations of the basic polyhedral units. However, while the relevance for NTE of transverse atomic motion is generally recognized, no definite correlation between RUMs and NTE can be established for all framework structures.[12] One of the main limitations to a satisfactory understanding of the origin of NTE in framework structures is the lack of direct experimental information on the expansion of distances between neighboring atoms, and on the actual degree of rigidity of polyhedral units.

Bragg diffraction experiments measure the distance between average atomic positions (*apparent bond length*[3] $|\langle \mathbf{r}_2 \rangle - \langle \mathbf{r}_1 \rangle|$) and its temperature variation, as well as the thermal parameters, which give the uncorrelated atomic mean square displacement amplitudes (MSDA).[13,14] The thermal expansion measured by diffraction corresponds to the one measured by macroscopic dilatometric techniques, but is in principle different from the average variation of inter-atomic distances (*true bond length* $\langle |\mathbf{r}_2 - \mathbf{r}_1| \rangle$), due to the presence of transverse vibrations. Attempts at assessing the *true* bond thermal expansion have been made in ZrW_2O_8 and in silicates,[15,16] by a refinement of Bragg spectra based on TLS models (translation, libration, and screw); these models, however, originally developed for molecular crystals, *a priori* assume the rigidity of the basic units.[14] A more direct method, based on the analysis of x rays or neutron total scattering, exploits the dependence of thermal diffuse scattering on correlation.[7,17,18]

A particularly effective and accurate approach to the local behavior of NTE materials is represented by extended x-ray absorption fine structure (EXAFS) spectroscopy.[19] Thanks to atomic selectivity and insensitivity to long-range order, EXAFS is complementary to Bragg diffraction, and an appealing alternative to total scattering. Actually, EXAFS can directly measure the true bond expansion and the *parallel* mean square relative displacement (MSRD) of selected pairs of neighboring atoms. By comparing the thermal expansions measured by EXAFS and Bragg diffraction, one can obtain the *perpendicular* MSRD,[20] whose knowledge can give significant insights into the local vibrations responsible for NTE. In an EXAFS study of ZrW_2O_8, Cao *et al.* focused

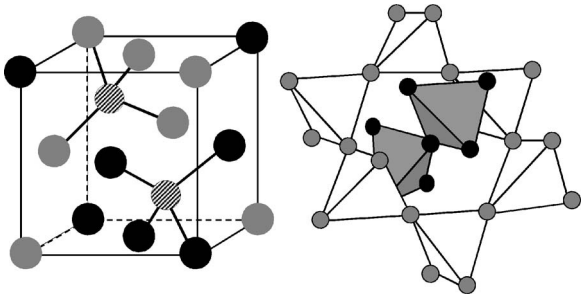

FIG. 1. The cuprite structure. Left: fcc unit cell of metal atoms (full circles), the two O atoms being represented by dashed circles. Right: partial sketch of the two interpenetrating networks of corner-sharing M_4O tetrahedra, whose M atoms are represented by black and grey circles, respectively.

their attention on the temperature dependencies of the *parallel* MSRDs of different atomic pairs, without however attempting to measure the corresponding bond thermal expansions.[21,22] Besides detecting a larger degree of rigidity of the WO_4 tetrahedra with respect to the ZrO_6 octahedra, those authors claimed that the Zr-O-W linkage is too rigid to allow the attribution of NTE to the relative rotation of rigid tetrahedral and octahedral structural units. Accordingly, they proposed a model for NTE based on a strong correlation of motion of each WO_4 tetrahedron with its three nearest ZrO_6 octahedra. Some of the EXAFS results of Cao *et al.*, as well as the model based on them, have been questioned by Tucker *et al.*, as contrasting with recent results of neutron total scattering measurement.[18]

ZrW_2O_8 is often considered as the archetypical NTE framework structure, and has received much attention by several authors in recent years. The presence of two kinds of slightly distorted structural units, WO_4 and ZrO_6, however, complicates the interpretation of experimental results. A simpler framework structure is exhibited by silver(I) and copper(I) oxides, Ag_2O and Cu_2O. Both compounds share the peculiar cubic *cuprite structure*, space group $Pn\bar{3}m$, made up by two interpenetrating lattices, one fcc of metal atom (M = Ag, Cu) and one bcc of oxygen atoms (O) (Fig. 1, left). Each M atom is linearly coordinated to two O atoms, while each O atom is tetrahedrally coordinated to four M atoms. Alternatively, the cuprite structure can be considered as a framework of two interpenetrating networks of corner-sharing undistorted M_4O tetrahedra, having the cristobalite-type topology (Fig. 1, right).

Cu_2O is a typical low thermal expansion material.[10] NTE below 200 K has been measured by laboratory x-ray powder diffraction[23] and subsequently confirmed by neutron[24] and synchrotron radiation x-ray diffraction.[25] The last two experiments[24,25] agree in reporting a positive thermal expansion from 300 to 650 K, and an anisotropic vibrational motion of copper atoms, more intense in the plane perpendicular to the O-Cu-O bond than along the bond. Transverse vibrations of this kind have been often correlated to NTE in several framework structures, such as β-quartz.[11]

Ag_2O has been comparatively little studied. A positive thermal expansion from 100 to about 500 K was reported in 1977 from laboratory x-ray diffraction.[26] The discrepancy with the behavior of Cu_2O led Taylor to question the reliability of thermal expansion data.[27] In 2003, accurate powder diffraction measurements showed that Ag_2O exhibits NTE from 40 to about 500 K (decomposition temperature).[6] NTE in Ag_2O has been recently confirmed by x-ray and neutron diffraction measurements performed up to 300 K,[28] which also evidenced a first-order phase transition below 35 K, previously detected by specific heat measurements.[29]

A strong NTE has been recently measured from 4 to 375 K in some members of the family $Zn_xCd_{1-x}(CN)_2$ by single-crystal x-ray diffraction.[30] These compounds exhibit the same framework structure of Cu_2O, where O is substituted by Zn or Cd and Cu is substituted by CN.

The great majority of the framework structures presents the cations at the center and the oxygen atoms at the corners of polyhedra, respectively. In cuprites, the situation is reversed, making these structures particularly well suited for EXAFS investigations. As a matter of fact, more reliable results can be obtained from the EXAFS spectra of relatively heavy cations than of oxygen atoms. In cuprites, by measuring EXAFS at the *K* edges of copper and silver, it is possible to obtain significant information not only about the nearest neighbors M-O distance, but also about the next-nearest-neighbors M-M distance. The 12 second-shell M atoms, although sharing the same distance to the absorbing atom, can be grouped into two sets: 6 atoms (Type A) belong to the same network of the absorbing atom, which are connected via a bridging nearest-neighbor oxygen atom, while the remaining 6 atoms (Type B) belong to the other network, and they do not share a nearest-neighbor oxygen atom with the absorbing atom.

Our first temperature-dependent EXAFS measurements performed on Ag_2O revealed a positive expansion of the Ag-O nearest-neighbors distance and a negative expansion of the average Ag-Ag next-nearest-neighbors distance.[31] Evidence was also found of a lack of rigidity of the basic tetrahedral units. These results were consistent with NTE measured by diffraction,[6] once the role of transverse vibrations was properly taken into account, but also suggested that a RUM model is inadequate to explain NTE in Ag_2O. On the basis of EXAFS results, NTE was tentatively attributed to the average approaching of Ag atoms belonging to different networks (Type B). That work demonstrated the effectiveness of EXAFS for NTE investigations, and stimulated extension of the study to complete and refine the interpretation of the underlying mechanisms.

In this paper, we will present a systematic study of thermal expansion and local lattice dynamics in Cu_2O and Ag_2O, based on a critical comparison of diffraction and EXAFS results. To this purpose, to integrate previous XRD results,[6] a set of neutron diffraction measurements has been expressly performed from 10 to 375 K on three synthetic Ag_2O powder samples of different origin and different purity degree. Only two of the samples (those with the highest and the lowest nominal impurity content, respectively) exhibited the same phase transition below 35 K as described in Refs. 28 and 29. An extensive account on the nature of the phase transition will be given elsewhere. Here we will only present the results for the sample which did not exhibit the phase transition, whose behavior is more directly comparable to

that of Cu_2O. Also EXAFS measurements on Cu_2O from 25 to 410 K and a new set of low-temperature measurements on Ag_2O, from 35 to 90 K, have been performed.

The paper is organized as follows. In Sec. II, a basic account is given of the main conceptual differences between the diffraction and EXAFS experiments, focusing on the effects of thermal motion (thermal expansion and mean square displacements). The diffraction and EXAFS experiments are described in Sec. III. Some relevant details of data analysis and the results of both diffraction and EXAFS are presented in Sec. IV. Sections V and VI are dedicated to discussion and conclusions, respectively.

II. EXAFS VERSUS DIFFRACTION

The complementarity of diffraction and EXAFS for the study of NTE materials can be traced back to the different nature of the scattering process and therefore to the different sensitivity to atomic thermal motion.

Powder diffraction experiments allow measuring the mean cell parameters and their temperature dependence, derived from the probed ensemble of coherently diffracting crystalline domains. For systems with atoms only in special positions, like cuprites, the distances $R=|\langle \mathbf{r}_2\rangle - \langle \mathbf{r}_1\rangle|$ between the average positions in space of any two atoms can be obtained from the cell parameters by direct proportionality. It has recently been shown that it is possible to measure the anisotropic displacement parameters (ADP) U_{ij} from Rietveld refinement of good quality powder diffraction data, even if this kind of refinement is more common from neutron data[32,33] than from x-ray data.[13,34] From the ADPs, the MSDA along selected directions can be calculated; in particular, here we are interested in the MSDA parallel and perpendicular to the M-O bond direction, $U_{\parallel}$ and $U_{\perp}$, respectively.

An EXAFS spectrum samples the one-dimensional distributions of single-scattering (SS) and multiple-scattering (MS) path-lengths within a few coordination shells of the absorbing atom.[35] For moderately disordered systems, it is convenient to parametrize the EXAFS signal of each scattering path in terms of the first cumulants C_i^* $(i=1,2,3,\ldots)$ of the distribution $\rho(r)$ of path-lengths.[20,36] The first cumulant corresponds to the mean of the distribution, $C_1^*=\langle r\rangle$, the second cumulant to the variance, $C_2^*=\langle (r-\langle r\rangle)^2\rangle$, and the third cumulant measures the asymmetry and is therefore related to the anharmonicity of the system. The SS contribution of the first coordination shell can often be singled out by Fourier filtering and separately analyzed. For outer shells, the SS contributions are generally entangled with MS effects, and their analysis is more complicated.

Let us consider here the meaning of cumulants for SS contributions; an extension to MS contribution can be found in Ref. 20. The second EXAFS cumulant C_2^* corresponds, to a very good approximation, to the *parallel* MSRD $\langle \Delta u_{\parallel}^2\rangle$ of the pair of absorber and backscatterer atoms,[37] where

$$\langle \Delta u_{\parallel}^2\rangle = \langle (\hat{\mathbf{R}}\cdot \mathbf{u}_a)^2\rangle + \langle (\hat{\mathbf{R}}\cdot \mathbf{u}_b)^2\rangle - 2\langle (\hat{\mathbf{R}}\cdot \mathbf{u}_a)(\hat{\mathbf{R}}\cdot \mathbf{u}_b)\rangle. \tag{1}$$

In Eq. (1), $\mathbf{u}_a$ and $\mathbf{u}_b$ are the instantaneous displacements of the absorber and backscatterer atoms, respectively, and $\Delta\mathbf{u}=\mathbf{u}_b-\mathbf{u}_a$. The first two terms on the right-hand side correspond to the uncorrelated MSDAs along the bond direction, $U_{\parallel}^a=\langle (\hat{\mathbf{R}}\cdot \mathbf{u}_a)^2\rangle$ and $U_{\parallel}^b=\langle (\hat{\mathbf{R}}\cdot \mathbf{u}_b)^2\rangle$, such as measured by diffraction. The last term is the *parallel* displacement correlation function (DCF).[38]

The first EXAFS cumulant $C_1^*=\langle |\mathbf{r}_2-\mathbf{r}_1|\rangle$ is the average distance between atomic positions, and it is in principle different from the distance between average positions R measured by diffraction. One can easily show that[37]

$$C_1^* = R + \langle \Delta u_{\perp}^2\rangle/2R, \tag{2}$$

where $\langle \Delta u_{\perp}^2\rangle$ is the *perpendicular* MSRD, say the projection of the total MSRD in the plane normal to the bond direction, defined as $\Delta u_{\perp}^2=\Delta u^2-\Delta u_{\parallel}^2$. Since $\langle \Delta u_{\perp}^2\rangle$ is positive, the EXAFS distance is larger than the crystallographic distance. In general, however, only *relative* values of distances can be obtained from EXAFS analysis with an accuracy sufficient for thermal expansion studies.[20] To the extent that $\langle \Delta u_{\perp}^2\rangle$ in Eq. (2) grows when temperature increases, the thermal expansion measured by EXAFS is larger than the crystallographic thermal expansion. Experimental measurements of the difference between EXAFS and diffraction thermal expansion have recently been made for the first coordination shells of germanium [39] and copper,[20] whence the perpendicular MSRDs could be estimated by inversion of Eq. (2).

The EXAFS analysis leads to the projections of the MSRD along the bond direction of a specific atomic pair and in the perpendicular plane, $\langle \Delta u_{\parallel}^2\rangle$ and $\langle \Delta u_{\perp}^2\rangle$, respectively. In case of axial symmetry around the bond direction, one can compare the EXAFS MSRDs with the corresponding MSDAs, $U_{\parallel}$ and $U_{\perp}$, measured by diffraction for both atoms. The parallel MSDAs $U_{\parallel}$ of the absorber and backscatterer atoms correspond to the first two terms on the right-hand side of Eq. (1). As far as the perpendicular parameters are concerned, $\langle \Delta u_{\perp}^2\rangle$ is the projection within the perpendicular plane, and should be divided by two before comparing with the $U_{\perp}$. In both parallel and perpendicular cases, the difference between the sum of the MSDAs of absorber and backscatterer atoms and the MSRD is due to correlation.

While the actual extent of correlation cannot be obtained solely from diffraction measurements, one can show, on the basis of probability theory, that the upper and lower bounds to correlation can be obtained from the MSDAs.[40] Accordingly, for parallel and perpendicular motions of a pair of atoms a and b, one has, respectively,

$$U_{\parallel}^a + U_{\parallel}^b - 2(U_{\parallel}^a U_{\parallel}^b)^{1/2} \le \langle \Delta u_{\parallel}^2\rangle \le U_{\parallel}^a + U_{\parallel}^b + 2(U_{\parallel}^a U_{\parallel}^b)^{1/2}, \tag{3}$$

$$U_{\perp}^a + U_{\perp}^b - 2(U_{\perp}^a U_{\perp}^b)^{1/2} \le \frac{\langle \Delta u_{\perp}^2\rangle}{2} \le U_{\perp}^a + U_{\perp}^b + 2(U_{\perp}^a U_{\perp}^b)^{1/2}, \tag{4}$$

where the left and right members of the inequalities refer to the relative displacements perfectly in phase and perfectly in opposition of phase, respectively.

The temperature dependence of the mean square displacements can be described with reasonable accuracy by a simple

phenomenological Einstein model, depending on only one parameter, the Einstein frequency $\omega_E = 2\pi\nu_E$ (or the Einstein temperature $\theta_E = \hbar\omega_E/k_B$). In the case of the absolute MSDAs measured by diffraction,

$$U = (\hbar/2m\omega_E)\coth(\hbar\omega_E/2k_BT), \quad (5)$$

where m is the atomic mass and ω_E is the frequency of oscillation of each atom around its equilibrium position. In the case of the *parallel* and *perpendicular* MSRDs measured by EXAFS for SS paths, the value $2m$ on the right-hand side prefactor of Eq. (5) is substituted by 2μ and μ, respectively, μ being the reduced mass of absorber and backscatterer atoms.[20] For the parallel MSRD, ω_E is the frequency of relative oscillation of absorber and backscatterer atoms, and can be connected to an effective bond-stretching force constant $\kappa = \mu\omega_E^2$. The Einstein frequencies best fitting the temperature dependence of the EXAFS MSRD are different for different coordination shells (and different from the Einstein frequencies of the MSDAs). Also for a given coordination shell, the Einstein frequencies best fitting the parallel and perpendicular MSRDs are generally different, owing to the anisotropy of the relative atomic motion.

III. EXPERIMENTS

Cu_2O powders 99.9% pure, purchased from Strem Chem. Inc., were used in x-ray diffraction and EXAFS experiments. Ag_2O powders 99% pure, purchased from Aldrich, were used in x-ray diffraction and EXAFS experiments, while powders 99.5% pure, purchased from Riedel-de-Haen, were used in neutron diffraction experiments. A check on the influence of purity was done with a third Ag_2O powder purchased from Aldrich, 99.99% pure.

A. Diffraction

X-ray powder diffraction measurements were done on Cu_2O from 5 to 630 K and on Ag_2O from 40 to 470 K.[6] Low temperature data (at and below 298 K) were measured with synchrotron radiation at the BM16 and ID 31 beamlines of ESRF (Grenoble, France), equipped with a closed-cycle liquid helium cryostat. The wavelength used was 0.4958 Å, calibrated against standard silicon, and the angular range was 5° to 60° 2θ, corresponding to a momentum transfer $4\pi\sin\theta/\lambda$ ranging from 1.1 to 12.7 $Å^{-1}$. High temperature data (at and above 298 K) were collected with a Philips Xpert $\theta-\theta$ diffractometer, equipped with a hot chamber (AHT, PAP1600), carefully calibrated for sample position and temperature.[41] Cu $K\alpha$ radiation was used, and the accelerating voltage and current of the x-ray tube were 40 kV and 40 mA, respectively. Data were collected in helium flux to avoid oxidation, from 27 to 95° 2θ, corresponding to a momentum transfer ranging from 3.7 to 8.12 $Å^{-1}$.

Neutron powder diffraction measurements were done on Ag_2O from 10 to 375 K, at 25 K steps, at the GEM beamline of the neutron spallation source ISIS (Rutherford Appleton Laboratories, UK). The GEM diffractometer is described elsewhere.[42] It encompasses eight banks of time of flight detectors, each one covering a limited range in scattering angle. A very high momentum transfer ($Q = 4\pi\sin\theta/\lambda \simeq 80$ $Å^{-1}$) can be achieved by merging the signals from all the detector banks.

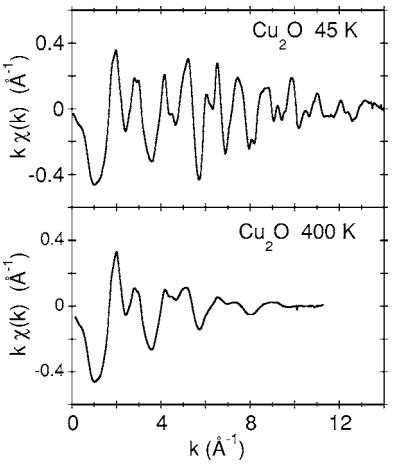

FIG. 2. EXAFS functions $k\chi(k)$ of Cu_2O at 45 and 400 K.

Room temperature refinement of the cell parameters of the starting materials were performed on a PANalytical X'Pert-Pro diffractometer, equipped with an X'Celerator detector, thus assuring an optimal signal/noise ratio for the subsequent full-profile analysis. Structural refinements were performed by the Rietveld method, using the program GSAS[43] with EXPGUI interface.[44]

B. EXAFS

A first set of transmission EXAFS measurements at the Ag K edge in Ag_2O had previously been done in the temperature range from 77 to 500 K at the BM-08 (Gilda) beamline of ESRF (Grenoble), utilizing a liquid nitrogen cryostat. Three spectra were also measured at and below 80 K in a liquid helium cryostat.[31] A new set of data, measured on the same beamline between 35 and 90 K, at steps of 5 K, has allowed us to increase the overall experimental information and reliably distinguish the Type A from Type B second-shell behavior in Ag_2O.

EXAFS measurements at the Cu K edge on Cu_2O have been done in the temperature range from 25 to 410 K at the BM-29 beamline of ESRF (Grenoble), utilizing a closed-cycle helium cryostat. Some spectra have been collected also at the BM-08 beamline, below 300 K.

Homogeneous samples of both compounds were prepared by depositing the corresponding powders on polytetraflouroethylene membranes, the thickness being chosen so as to have an absorption edge jump $\Delta\mu x \simeq 1$.

After a careful alignement of all spectra to within 0.1 eV or better, the EXAFS signals were obtained as $\chi(k) = [\mu(k) - \mu_1(k)]/\mu_0(k)$, where $\mu(k)$ is the experimental absorption coefficient, $\mu_1(k)$ is a spline polynomial best fitting the average behavior of $\mu(k)$, and $\mu_0(k)$ is a smooth Victoreen-like function with absolute values normalized to the absorption jump of each spectrum. Selected EXAFS functions $k\chi(k)$ are shown in Fig. 2 for Cu_2O and in Fig. 3 for Ag_2O.

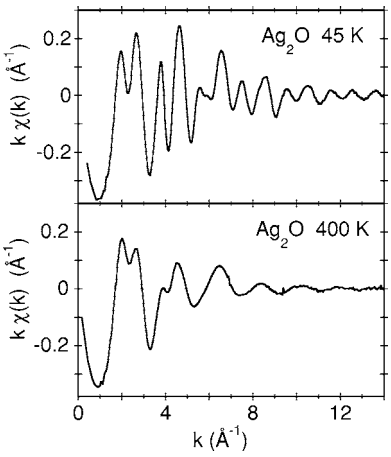

FIG. 3. EXAFS functions $k\chi(k)$ of Ag_2O at 45 and 400 K.

IV. RESULTS

A. Diffraction

The cell parameters a_0 of Cu_2O and Ag_2O, measured at 300 K by x-ray powder diffraction using silicon as standard reference (SRM 640c), are listed in Table I, together with the corresponding interatomic distances of the first four coordination shells. The value $a_0=4.27014(7)$ Å measured for Cu_2O is in good agreement with the value 4.2696 Å quoted by Wyckoff,[45] and 0.005 Å smaller than the value recently measured by Schäfer and Kirfel.[24] The value $a_0=4.7206(1)$ Å measured for Ag_2O is again in good agreement with the value 4.72 Å quoted by Wyckoff,[45] but smaller than the value of 4.7365 Å quoted by Kennedy *et al.*[28] The other two checked samples showed, on the other hand, a cell parameter $a_0=4.7361(1)$ Å that is much closer to the one published by Kennedy; this discrepancy can clearly be related to sample nonstoichiometry and therefore to the presence of the low temperature phase transition. The role of defects in Ag_2O will be discussed in detail in a separate paper.

The thermal expansions of the cell parameters of the two oxides are shown in Fig. 4. Cu_2O exhibits a negative thermal expansion between 9 and 240 K (linear thermal expansion coefficient $\alpha=-2.4\times10^{-6}$ K^{-1}), in good agreement with previous measurements by Schäfer and Kirfel.[24] Above room temperature, the thermal expansion is positive ($\alpha=1.6\times10^{-6}$ K^{-1}), but smaller than the one quoted by Schäfer and Kirfel. This small discrepancy may be attributed to the fact that different apparatuses are needed to perform the experiments at low and high temperature, therefore the different temperature calibration procedures and strategies may affect the true temperature estimation. Further, in our high temperature experiment a flat-plate diffraction geometry was used. Since this technique suffers from correlation between sample displacement and nominal temperature calibration, the data heavily rely on the theoretical values of the thermal expansion of the standard silicon lattice.

TABLE I. Cell parameters of Cu_2O and Ag_2O measured at 300 K by X-ray powder diffraction and corresponding interatomic distances of the first four coordination shells of the Cu or Ag atoms (M).

			Cu_2O	Ag_2O
Cell parameter (Å)		a_0	4.27014(7)	4.7206(1)
First shell	2 O	$\sqrt{3}a_0/4$	1.8490	2.0441
Second shell	12 M	$a_0/\sqrt{2}$	3.0194	3.3379
Third shell	6 O	$\sqrt{11}a_0/4$	3.5406	3.9141
Fourth shell	6 M	a_0	4.2701	4.7206

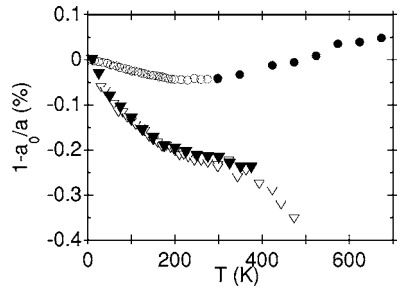

FIG. 4. Normalized percent variations of the cell parameters of Cu_2O (circles) and Ag_2O (triangles), where a_0 is the parameter measured at the lowest temperature. For Cu_2O, open and closed circles refer to x-ray measurements made with synchrotron radiation and laboratory tube, respectively (Ref. 25). For Ag_2O, open and closed triangles refer to x-ray (Ref. 6) and neutron measurements (present work), respectively. The uncertainty bars are smaller than the symbols size.

The neutron diffraction results for Ag_2O are in good agreement with the previous x-ray measurements,[6] as clearly shown in Fig. 4. The thermal expansion of Ag_2O is negative in the full temperature range explored, and significantly larger than in Cu_2O. Three temperature regions can roughly be singled out in Fig. 4, with different slopes: NTE is high below 150 K, where $\alpha\simeq-1.04\times10^{-5}$ K^{-1}, is reduced at intermediate temperatures ($\alpha\simeq-2.4\times10^{-6}$ K^{-1} around 250 K), and increases again at high temperature ($\alpha\simeq-9\times10^{-6}$ K^{-1}). Our results are in total disagreement with Srivastava *et al.*, who measured, by means of a laboratory diffractometer, a positive thermal expansion.[26] The overall agreement with Kennedy *et al.* is instead good.[28]. These authors could also measure the cell parameter below the phase transition temperature, due to the fact that the high temperature phase persisted in a large amount down to 5 K. In our previous x-ray measurements,[6] this was not possible, as the high temperature phase amount decreased deeply below 30 K, and eventually disappeared at 5 K. At higher temperatures, the thermal expansion data published by Norby *et al.*[46] showed NTE from 565 to 700 K, with a linear coefficient of about -2.85×10^{-5} K^{-1} up to about 630 K, from where it increases largely, and from where the authors observe a peak splitting. This NTE was measured while decomposing silver carbonate at high temperature in a closed sample holder (a boron glass capillary filled under CO_2 flux). It is worth noting that NTE in Ag_2O is comparable or even larger than in ZrW_2O_8, where $\alpha=-9.1\times10^{-6}$ K^{-1} between 10 and 300 K.[18]

Reliable thermal parameters could be obtained for Cu_2O from 5 to 300 K (x-ray synchrotron measurements), and for

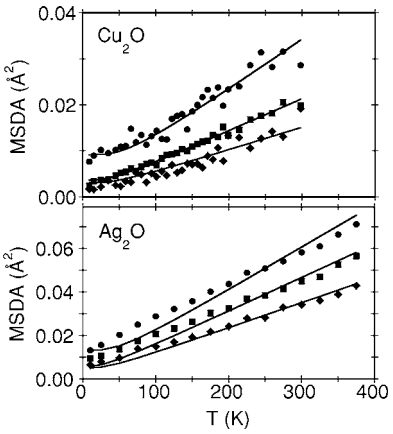

FIG. 5. MSDAs of copper or silver (diamonds $U_{\parallel}$, squares $U_{\perp}$) and oxygen (circles) in Cu_2O (upper panel) and Ag_2O (lower panel), as determined from diffraction. The continuous lines are best fitting Einstein models. Note the different vertical scales of the two graphs.

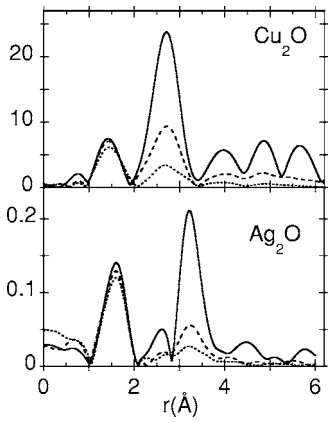

FIG. 6. Moduli of Fourier transforms of the EXAFS signals of Cu_2O and Ag_2O at 45, 200, and 400 K (continuous, dashed and dotted lines, respectively).

Ag_2O from 10 to 375 K (neutron measurements on the sample without low-temperature phase transition). In general, anisotropic atomic displacement parameters from powder diffraction data should be treated with great care, but here the excellent agreement with single crystal data in cuprite[13,25] proved the reliability of anisotropic thermal parameters from high-resolution powder diffraction data, at least in structurally simple compounds like cuprite. Because of the site symmetry constraints, only M atoms (M=Cu, Ag) are allowed anisotropic vibrations (anyway, $U_{11}=U_{22}=U_{33}$ and $U_{12}=U_{23}=U_{31}$). For both M atoms the parameters along the diagonal are positive, while those off-diagonal are small and negative. As a consequence, the thermal ellipsoids of copper and silver are flattened along the M-O direction, say $U_{\parallel}<U_{\perp}$ (Fig. 5). The temperature dependencies of all thermal factors are reasonably well fitted by Einstein models (the frequencies are listed in Table II), indicating that no significant contributions from static disorder are present and their small positive intercept at 0 K derives from zero-point motion alone. This is not the case in the other two Ag_2O samples with different nonstoichiometry, which clearly show an additional contribution derived from static disorder.[13] By comparing the thermal behavior of silver and copper, an important point is evident: the absolute values of the MSDAs of silver are always larger than those of copper at the same temperature, and also the difference between transverse and parallel motion are systematically larger in silver than in copper.

TABLE II. Einstein frequencies (THz) and corresponding temperatures (K) best fitting the temperature dependence of atomic MSDAs (from diffraction) and first- and second-shell MSRDs (from EXAFS). M = Cu, Ag.

			Cu_2O		Ag_2O	
			ν_E	θ_E	ν_E	θ_E
MSDA	M	$U_{\parallel}$	2.6	125	1.8	86
	M	$U_{\perp}$	2.2	106	1.6	77
	O	U_{iso}	3.4	163	2.8	134
MSRD	M-O	$\parallel$	14.9	715	10.2	490
	M-O	$\perp$	7.4	355	2.9	138
	M-M (average)	$\parallel$	3.1	149	1.7	82

B. EXAFS

The Fourier transforms (FT) of the EXAFS signals at selected temperatures are shown in Fig. 6 for both compounds. The FT features can be easily interpreted in terms of scattering paths, once the shortening of distances due to the phase-shift effect is taken into account. The peak between about 1 and 2 Å is due only to the contribution of the first coordination shell, made by two oxygen atoms (Table I). The structure between about 2 and 3.5 Å for Cu_2O (2 and 4 Å for Ag_2O) contains the SS contributions of the second and third coordination shells (Table I), as well as several MS contributions. The scattering paths of length smaller than 4 Å are listed in Table III for Cu_2O and schematically shown in Fig. 7.

It is immediately evident, from Fig. 6, that in both compounds the temperature effect is much weaker for the first than for the outer coordination shells. This evidence qualitatively suggests that the nearest-neighbors bond is much stiffer against stretching than the bond between farther atoms.

Different procedures were adopted for the analysis of the first and second coordination shells, respectively.

1. First-shell analysis

The first-shell signal was isolated by Fourier backtransform and analyzed by the *ratio method* within the framework of the cumulant expansion approach.[36,37] The lowest-temperature spectrum was used as reference for backscattering amplitude, phase shifts, and inelastic terms. As a result, relative values of the first three cumulants $\delta C_i^*(i=1-3)$ with

TABLE III. Scattering paths of effective length r_{eff} smaller than 4 Å in Cu_2O, as calculated by the FEFF8 code (Ref. 47). Two-leg paths 1, 2, and 4 correspond to single scattering from the first, second, and third coordination shells, respectively. Three- and four-leg paths correspond to multiple scattering. The last column lists the relative amplitude of the paths.

Index	Legs	Degeneracy	r_{eff} (Å)	Rel amp
1	2	2	1.8490	100.0
2	2	12	3.0194	162.2
3	3	12	3.3586	40.6
4	2	6	3.5406	57.8
5	3	2	3.6979	18.5
6	4	2	3.6979	8.1
7	4	2	3.6979	8.4
8	4	6	3.6979	10.9

respect to the reference were obtained. The ratio method, when applicable, allows a relatively easy visual estimate of the overall quality of experimental data and of the useful k range, which typically decreases when temperature increases. The possible influence of double electron excitations at the K edge of silver was checked by means of the GNXAS code[48] and found negligible for the present analysis.

In both compounds, the nearest-neighbors distance M-O, measured by the first cumulant C_1^* of the real distribution of distances, expands when temperature increases (Fig. 8, top panels). This effect is particularly strong in Ag_2O, where the average expansion coefficient is $\alpha \simeq +35 \times 10^{-6}\ \text{K}^{-1}$. In Cu_2O the effect is much weaker, and, owing to the dispersion of the data, can be appreciated only by looking at the average trend; the average expansion coefficient is $\alpha \simeq +7.5 \times 10^{-6}\ \text{K}^{-1}$. The difference between the positive expansion of the average distance measured by EXAFS and the negative expansion of the distance between average positions measured by diffraction is due, according to Eq. (2), to the increase of intensity of relative vibrations perpendicular to the bond direction.

Absolute values of the parallel MSRD $\langle \Delta u_{\parallel}^2 \rangle$ were obtained, according to a standard procedure,[49] by fitting an Einstein correlated model to the temperature dependence of the second cumulant. The perpendicular MSRD $\langle \Delta u_{\perp}^2 \rangle$ was instead estimated by calculating the difference between EXAFS and diffraction thermal expansions and, after multiplication by $2R$, again fitting to an Einstein model (Sec. II and Ref. 20). The best-fitting Einstein frequencies are listed in Table II.

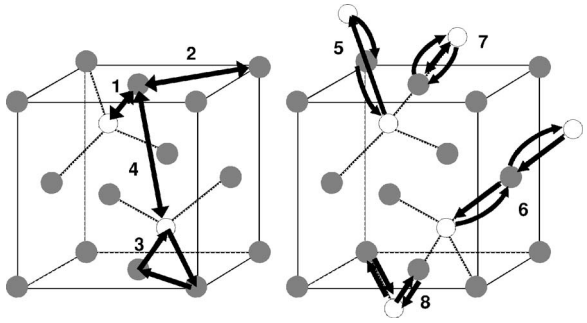

FIG. 7. Schematic representation of the first eight scattering paths in cuprites. Open and grey circles represent O and M atoms, respectively.

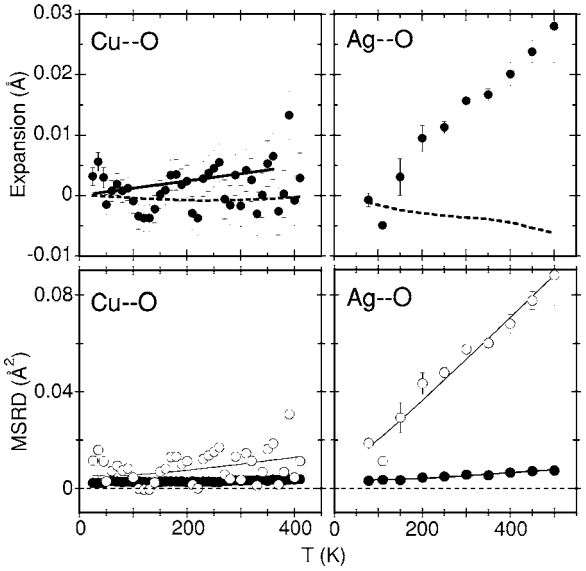

FIG. 8. First shell of M atoms (M=Cu,Ag) in Cu_2O (left) and Ag_2O (right). Top panels: Thermal expansion measured by EXAFS (dots) and diffraction (dashed lines); the continuous line for Cu_2O is a linear best fit to EXAFS data. Bottom panels: parallel MSRD $\langle \Delta u_{\parallel}^2 \rangle$ (closed circles) and perpendicular MSRD $\langle \Delta u_{\perp}^2/2 \rangle$ (open circles).

The parallel and perpendicular MSRDs define an ellipsoid of *relative* thermal displacements of O atoms with respect to M atoms, or vice versa. In Fig. 8 (bottom panels) the parallel and perpendicular MSRDs of Cu_2O and Ag_2O are compared. In both compounds, $\langle \Delta u_{\parallel}^2 \rangle < \langle \Delta u_{\perp}^2 \rangle /2$, say the ellipsoids of M-O relative motion are disk-shaped, like the ellipsoids of absolute motion of M atoms determined by diffraction experiments. The relative motion along the bond direction, measured by $\langle \Delta u_{\parallel}^2 \rangle$, is more intense in Ag_2O than in Cu_2O. A stronger difference is found for the relative motion perpendicular to the bond, so that the equatorial extension of the ellipsoids is larger in Ag_2O than in Cu_2O.

2. Second-shell analysis

A more refined analysis had to be done for obtaining information on the second shell. The scattering paths contributing to the second peak of FT have been singled out using the FEFF8 code[47] and are listed in Table III for Cu_2O. Indices 2 and 4 label the second- and third-shell SS paths, while index 3 labels the triangular MS path Cu-Cu′-O-Cu (Fig. 7, left). The MS paths labeled by the indices 5–8 contain only the Cu-O distance and are characterized by the same effective length (Fig. 7, right). To evaluate and compare the contributions of the different scattering paths 2–8, their EXAFS signals have been separately simulated by means of FEFF8. The corresponding FT are shown in Fig. 9. The contributions of paths 5–8 are much weaker than the contributions of paths

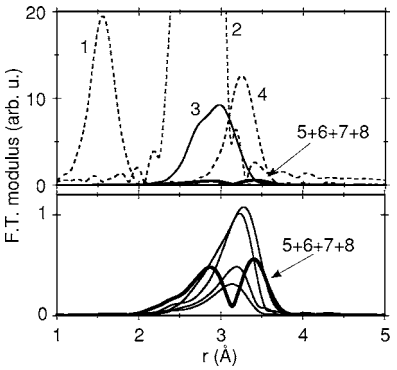

FIG. 9. Fourier transforms of the different scattering paths of Cu_2O listed in Table III. Dashed lines refer to SS paths, continuous lines to MS paths. Thermal disorder is not included. The bottom panel shows the contributions of paths 5–8 (thin lines) and the contribution of their sum (thick line). Only the global contribution of paths 5–8 is shown in the top panel.

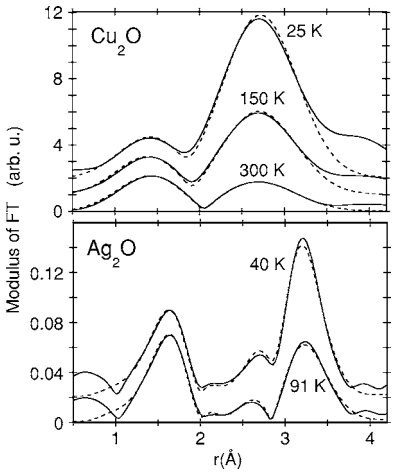

FIG. 10. Fourier transforms of EXAFS spectra of Cu_2O and Ag_2O at selected temperatures (full lines) and best fitting simulations (dashed lines). Low temperature spectra have been upward shifted to increase the readability.

2–4, and their mutual interference further reduces their overall influence. As a consequence, paths 5–8 have been considered negligible, for both Cu_2O and Ag_2O. Accordingly, only MS contributions corresponding to path 3 were taken into account in the subsequent analysis.

EXAFS spectra were simulated at different temperatures by the FEFF8 code, and the cumulant values were obtained through a nonlinear best-fit to experimental spectra, utilizing the FEFFIT code.[50] In a first attempt, the distinction between Type A and Type B second-shell atoms has been neglected, and the third-shell and MS contributions taken into account as perturbations, as in our previous work on Ag_2O (Ref. 31). A strong negative expansion is observed for the average Ag-Ag distance,[31] while for the average Cu-Cu distance the variations with temperature are within the uncertainty bars. In both compounds, the average second-shell parallel MSRD is much stronger than the first-shell one, as can be seen in Fig. 13 and from the best-fitting Einstein frequencies of Table II; this behavior quantitatively confirms the qualitative conclusions drawn from the observation that the second shell peaks of FT (Fig. 6) are very strongly reduced when temperature increases.

In a subsequent more refined analysis, it was assumed that the second-shell Type A and Type B atomic pairs may have different relative dynamics, as a consequence of the presence or absence, respectively, of a nearest-neighbor bridging oxygen. Actually, a different interaction between the two kinds of M-M pairs had to be considered by Kugel *et al.*[51] in order to satisfactorily reproduce the phonon dispersion curves of Cu_2O. Different thermal expansions and MSRDs for Type A and Type B were thus expected.

A completely unconstrained analysis of EXAFS, distinguishing the Type A and Type B distances and taking into account the cumulants of the relevant scattering paths (2, 3, and 4), led to meaningless and/or unstable solutions, due to the exceedingly large number of free parameters. The number of free parameters has then been reduced on the basis of the following simple geometrical considerations.

(a) Central atom M, first neighbors O, and second neighbors M′ of Type B are at the vertices of rectangular triangles, whose hypothenusa has the length of the third-shell distance. As a consequence, the first cumulant $C^*_{1,4}$ of the third shell (path 4) has been linked to the first cumulants $C^*_{1,1}$ of the first shell and $C^*_{1,2B}$ of the second shell Type B by the relation

$$C^*_{1,4} = [(C^*_{1,1})^2 + (C^*_{1,2B})^2]^{1/2}. \quad (6)$$

(b) The MS path 3 corresponds to a M-O-M″-M triangle within a M_4O tetrahedron, M″ being a Type A second neighbor. As a consequence, the length of the MS path 3 has been expressed as

$$C^*_{1,3} = 2C^*_{1,1} + C^*_{1,2A}. \quad (7)$$

Similar simple links based on geometrical considerations could not be found for the second cumulants, in view of the difficulty of *a priori* estimating the correlation effects. A set of simulations has then been performed, imposing to the ratio $C_{2,4}/C_{2,2B}$ (third shell path) different values varying from 0.75 to 3, and to the ratio $C_{2,3}/C_{2,2A}$ (MS path) different values varying from 0.5 to 2.5. The third cumulants of all scattering paths had anyway to be neglected, in order to guarantee the stability of the fitting procedure.

Initial values of distances were set to the crystallographic values, with $C^*_{1,2A}=C^*_{1,2B}$, and initial values of second cumulants were set to zero. The fits were made in real space (Fig. 10), including the first-shell peak. The values of energy shift E_0 and inelastic reduction factor S_0^2, left free in a first trial analysis, slightly varied as a function of temperature. Average values of E_0 and S_0^2 were then calculated and maintained fixed in a further analysis, leading to a substantial reduction of the uncertainty bars and of the scattering of cumulant values as a function of temperature.

In the case of Cu_2O, this analysis was made up to 300 K. The results are shown in Fig. 11. The variations of interatomic distances and parallel MSRDs of both Type A and Type B Cu-Cu pairs are clearly dependent on the values of the imposed ratios $C_{2,4}/C_{2,2B}$ and $C_{2,3}/C_{2,2A}$. It is nevertheless possible to distinguish a different behavior for the two

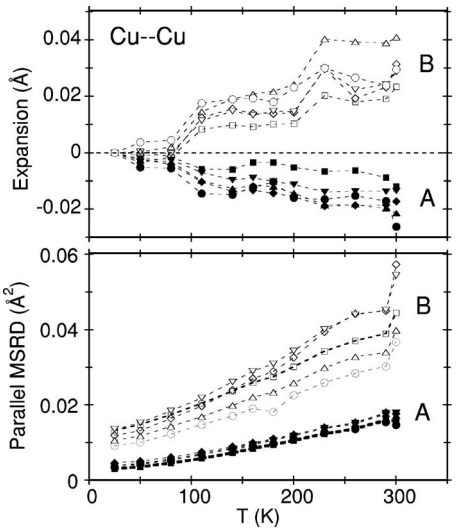

FIG. 11. Thermal expansion (top panel) and parallel MSRD (bottom panel) of the Cu-Cu second-shell distance in Cu_2O, for different values of the ratios $C_{2,4}/C_{2,2B}$ and $C_{2,3}/C_{2,2A}$: Closed symbols refer to Type A distances, open symbols to Type B.

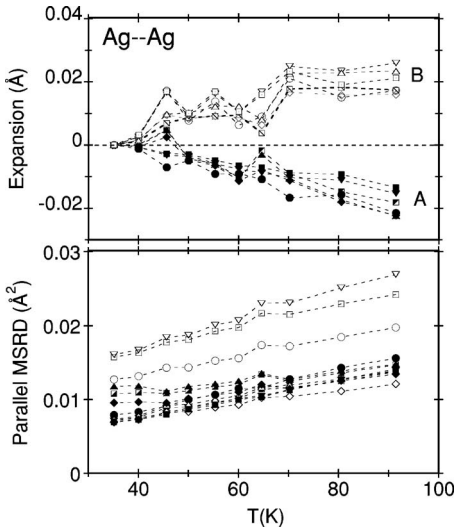

FIG. 12. Thermal expansion (top panel) and parallel MSRD (bottom panel) of the Ag-Ag second-shell distance in Ag_2O, for different values of the ratios $C_{2,4}/C_{2,2B}$ and $C_{2,3}/C_{2,2A}$: Closed symbols refer to Type A distances, open symbols to Type B.

kinds of Cu–Cu pairs: the Type A distance, say the distance between Cu atoms at the corners of the same Cu_4O tetrahedron, always decreases when temperature increases, while the Type B distance, say the distance between Cu atoms belonging to two different networks, always increases. Besides, the parallel MSRD of Type B atomic pairs is higher than the parallel MSRD of Type A pairs. The values of Type B parallel MSRD are by far more sensitive to the ratios $C_{2,4}/C_{2,2B}$ and $C_{2,3}/C_{2,2A}$. It should be remembered that the ratio between two quantities behaving according to Einstein models, like the MSRDs, is asymptotically constant only at high temperatures, unless the two models have the same frequency. The constraint of fixed ratios between MSRDs is thus expected to introduce inaccuracies, in particular at low temperatures. The spread of values of thermal expansions and parallel MSRDs corresponding to different values of the ratios $C_{2,4}/C_{2,2B}$ and $C_{2,3}/C_{2,2A}$ can reasonably be assumed as a rough estimate of their uncertainty.

In the case of Ag_2O, the analysis was possible only from 40 to 90 K, on the new set of specifically measured high quality data (Fig. 12). The results are in qualitative agreement with those of Cu_2O for what concerns thermal expansion: Clearly, Type A distance contracts and Type B distance increases. The situation is less obvious for the parallel MSRDs. Actually, the values of the Type B parallel MSRD are much more sensitive to the ratios $C_{2,4}/C_{2,2B}$ and $C_{2,3}/C_{2,2A}$ than in Cu_2O, and for low values of $C_{2,4}/C_{2,2B}$ and high values of $C_{2,3}/C_{2,2A}$ they merge with the values of Type A MSRD. The spread of MSRD data can again be attributed to the roughness of the hypothesis of constant ratios between MSRDs, enhanced by the low temperature of Ag_2O data.

To perform an independent qualitative test of the above-noted results, the FEFFIT program was run neglecting the third shell and MS contributions, but imposing that the Type A and Type B second cumulants had different values. The result of the best-fit procedure is again that the distance having the smaller second cumulant undergoes negative expansion, and vice versa, the behavior being qualitatively independent of the ratio $C^*_{2,B}/C^*_{2,A}$ within the reasonable range from 1.5 to 3.

V. DISCUSSION

The lattice thermal expansion, as measured by diffraction (Fig. 4), is negative in both compounds below about 250 K, NTE being however six times larger in Ag_2O than in Cu_2O. Above 250 K, in Cu_2O the positive contribution to thermal expansion due to anharmonicity prevails over the negative contribution. The overall behavior of Cu_2O is qualitatively similar to that of tetrahedrally coordinated semiconductors affected by NTE, like Ge or CuCl. On the contrary, in Ag_2O the negative expansion extends up to about 500 K (decomposition temperature), and the behavior is more similar to that of other framework structures, like ZrW_2O_8 and $Zn(CN)_2$. The low-temperature thermal expansion coefficients of the cell parameters of different framework-structured systems are compared in Table IV: NTE in Ag_2O is four times stronger than in Cu_2O, comparable to that in ZrW_2O_8 (Ref. 5) and quartz,[17] and about two times weaker than in $Zn(CN)_2$ (Ref. 7).

The MSDAs, measured up to 300 K in Cu_2O and 375 K in Ag_2O (Fig. 5), exhibit a common behavior: the MSDA of

TABLE IV. Low-temperature ($T<200$ K) thermal expansion coefficients (10^{-6} K^{-1}) for cell parameters and nearest-neighbors bonds Cu-O, Ag–O, Zn–C/N, and Si–O.

	Cu_2O	Ag_2O	ZrW_2O_8 (Ref. 5)	$Zn(CN)_2$ (Ref. 7)	Quartz (Ref. 17)
Cell	−2.4	−10.4	−9.1	−19.8	−7.8
Bond	+7.5	+35		+10	+2.2

oxygen atoms is larger and isotropic, the MSDA of the metal atoms is anisotropic, characterized by stronger vibrations in the plane perpendicular to the O-M-O linkage than in the parallel direction. This kind of anisotropy is often qualitatively connected to NTE effects. Thus, since the overall intensity of thermal vibrations in Ag_2O is about twice the intensity in Cu_2O, the difference is obviously related to the different behavior of NTE in the two compounds.

A deeper understanding is gained from EXAFS results and their comparison with diffraction results. EXAFS is able to measure the true expansion of average distances between nearest-neighbors, M-O, and next-nearest-neighbors, M-M. The nearest-neighbor M-O thermal expansion, directly measured by EXAFS, is positive in both compounds in all the explored temperature ranges (Fig. 8, top panels). This behavior is not surprising, and can be considered direct evidence of the anharmonic character of the interaction potential. Less obvious is the large difference between the positive coefficients (from EXAFS) and the negative coefficients (from Bragg diffraction): $\Delta\alpha=\alpha_{\mathrm{EXAFS}}-\alpha_{\mathrm{diff}}\simeq 9.9\times10^{-6}\ \mathrm{K}^{-1}$ and $45.4\times10^{-6}\ \mathrm{K}^{-1}$ for Cu_2O and Ag_2O, respectively. It is worth noting that the system with the largest NTE (say Ag_2O) is characterized also by the largest positive nearest-neighbor expansion.

Large differences between positive bond expansion coefficients (from diffuse scattering) and negative cell expansion coefficients (from Bragg diffraction) have been found also in quartz[17] and in $Zn(CN)_2$ (Ref. 7), as shown in Table IV.

The difference between EXAFS and diffraction expansion is due to the effect of perpendicular relative vibrations. The anisotropy of the *relative* nearest-neighbors motion measured by EXAFS (Fig. 8, bottom panels) is qualitatively similar to the anisotropy of the *absolute* motion measured by diffraction (Fig. 5), but quantitatively much stronger. The disk-shaped ellipsoid of relative thermal motion is much more flat than the ellipsoid of absolute thermal motion of M atoms.

The sensitivity of EXAFS to correlation is evidenced in Fig. 13 by the direct comparison between the MSRDs measured by EXAFS (diamonds) and the uncorrelated MSDAs measured by diffraction (circles). The correlation of vibrations of nearest-neighbors M and O atoms is very strong along the bond direction (Fig. 13, top panels). The parallel MSRD (diamonds) in both compounds is very similar to the lower limit of Eq. (3) (up triangles), which corresponds to an in-phase motion of the two atoms. This suggests that the M-O bond is very stiff against stretching. In the perpendicular directions (Fig. 13, middle panels), the correlation is less strong, suggesting that the M-O bond is less stiff against bending than against stretching, and that the flattening of the relative ellipsoids with respect to the M absolute ellipsoids is mainly due to the correlation along the bond direction. The perpendicular correlation is weaker in Ag_2O than in Cu_2O, and this again is connected to a larger NTE effect in Ag_2O.

The stiffness against stretching also characterizes the bond between metal atoms and neighboring oxygen atoms in ZrW_2O_8, where Cao *et al.*[22] found relatively high Einstein temperatures by best fitting the parallel MSRDs; the values $\theta_D=962$ and 493 K for the W-O and Zr-O bonds, respectively, can be compared with those found in the present work for the Cu-O and Ag-O bonds, 715 and 490 K, respectively (Table II).

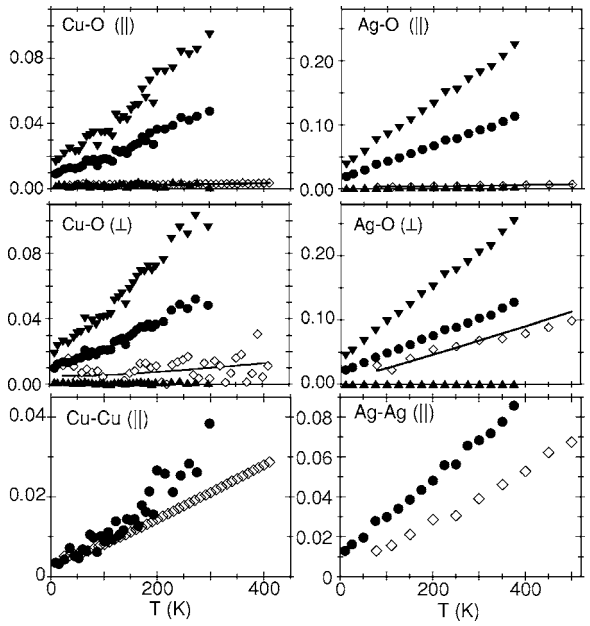

FIG. 13. Comparison between the sums of uncorrelated MSDAs (circles, from diffraction) and the correlated MSRDs $\langle\Delta u_{\parallel}^2\rangle$ or $\langle\Delta u_{\perp}^2\rangle/2$ (diamonds, from EXAFS) for first-shell parallel (top panels), first-shell perpendicular (middle panels), and second-shell parallel (bottom panels) displacements. Left and right panels refer to Cu_2O and Ag_2O, respectively. The continuous lines are Einstein models best-fitting the EXAFS MSRDs. Inverted triangles and triangles in the first-shell panels are the maxima and minima values of MSRDs estimated from diffraction data through Eqs. (3) and (4).

The anisotropy of nearest-neighbors relative motion was detected by EXAFS also in germanium[39] and AgI,[52] and it is probably characteristic of tetrahedrally bonded semiconductors, where NTE is present, albeit often in limited temperature ranges. However, while in Cu_2O and Ag_2O the anisotropy of the relative motion is accompanied by a weaker anisotropy of the ellipsoids of absolute thermal motion of metal atoms (Fig. 5), in germanium and AgI the absolute thermal ellipsoids, when anharmonicity effects are neglected, reduce to spheres. These findings suggest that negative contributions to thermal expansion should be connected to perpendicular relative, rather than absolute, thermal motion. In this respect, EXAFS and total scattering are expected to play a crucial role for understanding the local origin of NTE.

Let us now consider the second-shell EXAFS results. In both compounds, a different behavior is found for the two kinds of M-M next-nearest-neighbor pairs, Type A (sharing an O atom as first neighbor and belonging to the same network of tetrahedra) and Type B (belonging to two different networks of tetrahedra). The different interaction between the two kinds of M-M pairs had already been stressed by Kugel *et al.*,[51] According to EXAFS, the distance between Type A pairs of metal atoms (corresponding to the edge of M_4O tetrahedra) contracts when temperature increases, while the distance between Type B pairs increases (Figs. 11 and 12, top panels). This result suggests a rather complex local behavior. The presence of empty sites in the cuprite structure, with respect for example to zincblende, is reasonably expected to play a relevant role in the extension of NTE over

large temperature intervals. The attribution of NTE to a progressive reduction of the average Type B M-M distance induced by the presence of empty sites, which had tentatively been proposed in our previous work,[31] is however inconsistent with the present results. The contraction of the average length of the edges of M_4O tetrahedra (Type A), monitored by EXAFS, corresponds to an intranetwork contribution to NTE, while the internetwork M-M distances (Type B) actually undergo positive expansion. The possible further contribution to NTE due to intranetwork relative rotations of M_4O tetrahedra involves larger M-M distances and escapes detection from EXAFS.

Also the second-shell parallel MSRDs are different for Type A and Type B metal pairs (Figs. 11 and 12, bottom panels). The Type A MSRDs are smaller, as expected from the presence of a bridging oxygen atom nearest-neighbor, which contributes to a stiffening of the Type A bond with respect to Type B. The high values of Type B parallel MSRDs are connected to the high values of first-shell perpendicular MSRDs, although a quantitative relation cannot be easily determined, in view of the unknown extent of correlation.

The second-shell parallel MSRDs (both Type A and Type B) are much larger than the first-shell parallel MSRDs, indicating a much weaker M-M than M-O correlation. The reduced extent of second-shell parallel correlation is evident also in Fig. 13 (bottom panels), where the average parallel MSRDs, obtained in an extended temperature range without distinguishing Type A from Type B distances, are compared with the corresponding sums of MSDAs (the MSRD of Ag_2O is from Ref. 31).

The relatively high values of Type A MSRDs indicate that the M_4O tetrahedra are strongly deformed by thermal motion. This result confirms the inadequacy of a RUM model, based on the rotation of rigid or quasirigid structural units, to explain the NTE behavior of cuprites. The stiffness of the M-O bonds, together with the high values of first-shell perpendicular MSRD and second-shell parallel Type A MSRD, suggest that a possible dynamical model explaining NTE in cuprites should be based on the more flexible idea of rigid M-O rods.

Let us again consider the difference between EXAFS and diffraction results. A common feature is evident for both the first and the second coordination shells of both compounds: the positive or negative expansions of selected bonds measured by EXAFS are much larger, in absolute values, than the average thermal expansions measured by diffraction. This fact has probably to do with the relatively open structure of cuprite, which allows the possibility of large thermal movements inducing both positive and negative expansion of local distances. The average effect of these movements, measured by diffraction, is however much weaker than the effect of each one taken separately. A full quantitative connection between the EXAFS picture, distinguishing three different interatomic distances (M-O and M–M Type A and Type B), and the average expansion measured by diffraction is far from trivial. A key role in the difference between EXAFS and diffraction expansions is played by the correlation term in MSRDs and its temperature dependence, whose evaluation for all the relevant interatomic distances would require an accurate knowledge of the dynamical matrix and its eigenvectors throughout the entire Brillouin zone.

Diffraction and EXAFS results below about 300 K show a remarkable qualitative similarity between Cu_2O and Ag_2O. A common origin of NTE below 300 K can thus reasonably be postulated, the quantitative difference between expansion coefficients being amenable to the difference in amplitude and anisotropy of thermal motions. The quality of experimental data is lower at higher temperatures, and consequently the amount of obtainable information is smaller. It is thus difficult, on the basis of the present structural measurements, to give a satisfactory quantitative explanation of the different behavior of the two compounds at high temperature (positive expansion for Cu_2O, negative for Ag_2O).

Concerning the details of the electronic structure and chemical bonding in the two compounds, a large number of theoretical and experimental studies on the charge density in Cu_2O have been performed in the past because of the unusual linear O-Cu-O bond, the specific claims of symmetry forbidden diffraction effects, and the continuing debate on the charge accumulation in the interstitial regions (see, for example, Refs. 53–57, and references therein). Much less has been published on Ag_2O because of the lack of suitable samples for single crystal diffraction, and because of the difficulties in the adequate modeling of the electronic structure of silver. Perusal of tabulated values for the bond dissociation energy indicates 243 and 213 kJ mol^{-1} for the Cu-O and Ag-O pairs, respectively,[58] which points toward stronger interatomic interactions in Cu_2O than in Ag_2O. The linear features of the O-M-O bonds—implying a certain degree of covalency of the bond, a s-d_{z^2} hybridization, and the need for M_2M bonding to stabilize the interpenetrated framework—have been largely discussed in the literature for cuprite. Further, recent calculations performed on both compounds by hybrid Hartree-Fock and density functional-Hamiltonians[59] seem to indicate that the charge density at the (3,-1) saddle points along the Ag-O and Ag-Ag bonds show about a third of the charge density present in Cu_2O at the same points. Curiously, the estimates of the bond strengths performed by Einstein fit of the MSRDs in Table II also show similar reduction of the Einstein frequencies of the M-O and M-M bonds in Ag_2O with respect to Cu_2O. The difference in the electronic density and in the bond strength between Ag_2O and Cu_2O are related to the larger vibration amplitudes of the Ag atoms with respect to the Cu atoms, observed by EXAFS and diffraction at all temperatures. Weaker bonds and larger transverse motion of the Ag atoms seems to be the cause of the NTE of Ag_2O in the whole temperature range, similar to what happens in ZrW_2O_8. Similar NTE effects, which are present in Cu_2O in the low temperature range, are apparently overtaken above room temperature by anharmonic effects dominating the Cu vibrational behavior[13] and the lattice expansion of Cu_2O at high temperature is positive.

At last, let us shortly comment on the comparison between the present EXAFS results on Cu_2O and Ag_2O and the diffuse scattering results on $Zn(CN)_2$ of Ref. 7. Both techniques measure the true bond thermal expansion; while however the analysis of the pair distribution function is based on the Gaussian approximation, the cumulant analysis of EXAFS takes into account the distribution asymmetry, thus

guaranteeing, at least in principle, a better accuracy. In any case, the relation between real and apparent thermal expansions, due to the effect of perpendicular vibrations, is different in the two types of compounds, since different is the bridge between tetrahedral structural units: one M atom (M =Cu, Ag) in cuprites, two atoms (C-N) in $Zn(CN)_2$. As a consequence, one can reasonably expect a smaller difference between true and apparent bond expansions in the latter case. Finally, EXAFS on cuprites probes the environment of the M bridging atoms; by measuring the second shell M-M correlation, EXAFS is a direct test of the rigidity of tetrahedral units, and indirectly of the soundness of RUM models.

VI. CONCLUSIONS

An investigation of the thermal expansion of Cu_2O and Ag_2O has been performed by a joint use of powder diffraction and EXAFS. Both compounds share the relatively simple cuprite structure. A negative expansion of the cell parameter has been measured by diffraction from 9 to 240 K in Cu_2O and up to 470 K in Ag_2O. Cu and Ag atoms undergo anisotropic thermal displacements.

EXAFS at the *K* edges of Cu and Ag atoms shows that the nearest neighbor M-O distance undergoes positive expansion, and the relative thermal motion is characterized by a relative perpendicular to parallel anisotropy much stronger than the absolute one of Cu and Ag atoms. The second-shell analysis allows one to distinguish the different behavior of M-M pairs belonging to the same or to different networks of M_4O tetrahedra, the first ones reducing, the second ones increasing their distance when temperature increases. The intense relative motion of second-shell M-M atomic pairs indicates a strong deformation of M_4O tetrahedra, ruling out the possibility of explaining NTE in cuprite structures by a simple RUM model based on the movement of rigid or quasirigid structural units.

The local behavior of NTE materials can be rather complex, the correlation of vibrational motion playing a key role. EXAFS is a powerful tool, complementary to diffraction, owing to the sensitivity to correlation and the ability of measuring the true expansion of selected bonds, which in turn allows determining the perpendicular MSRD.

The inadequacy of RUM models stimulates the development of alternative phenomenological models, based on less stringent hypotheses. The relevance of the correlation terms points to the necessity of a stronger theoretical support, leading to reliable estimates of the eigenvectors of the dynamical matrix and of the anharmonicity effects. Improved ab initio calculations of the electronic densities could also contribute to yield new insights into the nature of the chemical bonds and of the different NTE behavior of Cu_2O and Ag_2O at high temperatures.

ACKNOWLEDGMENTS

We acknowledge the European Synchrotron Radiation Facility (ESRF) for provision of synchrotron radiation facilities. We are grateful to F. Bardelli, F. D'Anca, F. Lamanna, M. Brunelli, M. Borowski, and A. Fitch for experimental assistance on the ESRF beamlines BM08-Gilda, BM16, BM29, and ID31. P.G. Radaelli and W.I.F. (Bill) David are acknowledged for their help during neutron data collection and for many helpful discussions. This work has been partially supported by INFM Project Nos. 08-01-290 and 08-01-648 and by ESRF Project Nos. CH-1250, CH-1501, and HS-1720. A.S. acknowledges the support of the Provincia Autonoma di Trento, through the LOTHEX project at IFN-CNR.

*Electronic address: paolo.fornasini@unitn.it

[1] T. F. Smith and G. K. White, J. Phys. C **8**, 2031 (1975).
[2] G. K. White, Contemp. Phys. **34**, 193 (1993).
[3] G. D. Barrera, J. A. Bruno, T. H. K. Barron, and N. L. Allan, J. Phys.: Condens. Matter **17**, R217 (2005).
[4] T. H. K. Barron, in *Thermal Expansion of Solids*, CINDAS Data Series on Material Properties, Vol. I-4, edited by C. Y. Ho (1998).
[5] T. A. Mary, J. S. O. Evans, T. Vogt, and A. W. Sleight, Science **272**, 90 (1996).
[6] W. Tiano, M. Dapiaggi, and G. Artioli, J. Appl. Crystallogr. **36**, 1461 (2003).
[7] K. W. Chapman, P. J. Chupas, and C. J. Kepert, J. Am. Chem. Soc. **127**, 15630 (2005).
[8] J. R. Salvador, F. Guo, T. Morgan, and M. G. Kanatzidis, Nature (London) **425**, 702 (2003).
[9] A. Sleight, Nature (London) **425**, 674 (2003).
[10] R. Roy, D. K. Agrawal, and H. A. McKinstry, Annu. Rev. Mater. Sci. **19**, 59 (1989).
[11] V. Heine, P. R. L. Welche, and M. T. Dove, J. Am. Ceram. Soc. **82**, 1793 (1999).
[12] J. Tao and A. Sleight, J. Solid State Chem. **173**, 442 (2003).
[13] G. Artioli, in *Energy Modelling in Minerals*, EMU Notes in Mineralogy Vol. 4, edited by C. M. Gramaccioli (Eötvös University Press, Budapest, 2002), pp. 389–405.
[14] B. T. M. Willis and A. W. Pryor, *Thermal Vibrations in Crystallography* (Cambridge University Press, New York, 1975).
[15] J. S. O. Evans, W. I. F. David, and A. W. Sleight, Acta Crystallogr., Sect. B: Struct. Sci. **55**, 333 (1999).
[16] R. Downs, G. Gibbs, K. Bartelmehs, and J. M. B. Boisen, Am. Mineral. **77**, 751 (1992).
[17] M. G. Tucker, M. T. Dove, and D. A. Keen, J. Phys.: Condens. Matter **12**, L425 (2000).
[18] M. G. Tucker, A. L. Goodwin, M. T. Dove, D. A. Keen, S. A. Wells, and J. S. O. Evans, Phys. Rev. Lett. **95**, 255501 (2005).
[19] T. M. Hayes and J. B. Boyce, Solid State Phys. **37**, 173 (1982).
[20] P. Fornasini, S. a Beccara, G. Dalba, R. Grisenti, A. Sanson, M. Vaccari, and F. Rocca, Phys. Rev. B **70**, 174301 (2004).
[21] D. Cao, F. Bridges, G. Kowach, and A. Ramirez, Phys. Rev. Lett. **89**, 215902 (2002).
[22] D. Cao, F. Bridges, G. Kowach, and A. Ramirez, Phys. Rev. B **68**, 014303 (2003).

[23] M. Ivanda, D. Waasmaier, A. Endriss, J. Ihringer, A. Kirfel, and W. Kiefer, J. Raman Spectrosc. **28**, 487 (1997).
[24] W. Schäfer and A. Kirfel, Appl. Phys. A: Mater. Sci. Process. **74**, S1010 (2002).
[25] M. Dapiaggi, W. Tiano, G. Artioli, A. Sanson, and P. Fornasini, Nucl. Instrum. Methods Phys. Res. B **200**, 231 (2003).
[26] S. P. Srivastava, R. C. Srivastava, and S. D. Pandey, J. Phys. Soc. Jpn. **43**, 1463 (1977).
[27] D. Taylor, Br. Ceram. Trans. J. **84**, 9 (1985).
[28] B. J. Kennedy, Y. Kubota, and K. Kato, Solid State Commun. **136**, 177 (2005).
[29] K. S. Pitzer, R. E. Gerkin, L. V. Gregor, and C. N. R. Rao, Pure Appl. Chem. **2**, 211 (1960).
[30] A. L. Goodwin and C. J. Kepert, Phys. Rev. B **71**, 140301 (2005).
[31] S. a Beccara, G. Dalba, P. Fornasini, R. Grisenti, A. Sanson, and F. Rocca, Phys. Rev. Lett. **89**, 025503 (2002).
[32] W. I. F. David, R. M. Ibberson, G. A. Jeffrey, and J. R. Ruble, Physica B **180-181**, 597 (1992).
[33] B. J. Kennedy, Acta Crystallogr., Sect. C: Cryst. Struct. Commun. **51**, 790 (1995).
[34] M. Dusek, V. Petrcek, M. Wunschel, R. E. Dinnebier, and S. van Smaalen, J. Appl. Crystallogr. **34**, 398 (2001).
[35] J. Rehr and R. Albers, Rev. Mod. Phys. **72**, 621 (2000).
[36] G. Bunker, Nucl. Instrum. Methods Phys. Res. **207**, 437 (1983).
[37] P. Fornasini, F. Monti, and A. Sanson, J. Synchrotron Radiat. **8**, 1214 (2001).
[38] G. Beni and P. M. Platzman, Phys. Rev. B **14**, 1514 (1976).
[39] G. Dalba, P. Fornasini, R. Grisenti, and J. Purans, Phys. Rev. Lett. **82**, 4240 (1999).
[40] W. R. Busing and H. A. Levy, Acta Crystallogr. **17**, 142 (1963).
[41] M. Dapiaggi, G. Artioli, and L. Petras, Rigaku J. **19**, 1 (2002).
[42] A. C. Hannon, Nucl. Instrum. Methods Phys. Res. A **551**, 88 (2005).
[43] A. C. Larson and R. B. V. Dreele, Los Alamos National Laboratory, Report No. LAR 86–748, 2000.
[44] B. H. Toby, J. Appl. Crystallogr. **34**, 210 (2001).
[45] R. W. G. Wyckoff, *Crystal Structures* (Wiley, New York, 1963), Vol. 1.
[46] P. Norby, R. Dinnebier, and A. N. Fitch, Inorg. Chem. **41**, 3628 (2002).
[47] A. Ankudinov, B. Ravel, J. Rehr, and S. Conradson, Phys. Rev. B **58**, 7565 (1998).
[48] A. Filipponi, A. D. Cicco, and C. R. Natoli, Phys. Rev. B **52**, 15122 (1995).
[49] G. Dalba and P. Fornasini, J. Synchrotron Radiat. **4**, 243 (1997).
[50] M. Newville, B. Ravel, J. Rehr, E. Stern, and Y. Yacoby, Physica B **208-209**, 154 (1995).
[51] G. E. Kugel, C. Carabatos, and W. Kress, in *Ab Initio Calculation of Phonon Spectra*, edited by J. T. Devreese (Plenum, New York, 1983), pp. 101–115.
[52] G. Dalba, P. Fornasini, R. Gotter, and F. Rocca, Phys. Rev. B **52**, 149 (1995).
[53] R. Restori and D. Schwarzebach, Acta Crystallogr., Sect. B: Struct. Sci. **42**, 201 (1986).
[54] J. Zuo, M. Kim, M. O'Keeffe, and J. Spence, Nature (London) **401**, 49 (1999).
[55] T. Lippman and J. R. Schneider, Acta Crystallogr., Sect. A: Found. Crystallogr. **56**, 575 (2000).
[56] S. G. Wang and W. H. E. Schwarz, Angew. Chem., Int. Ed. **39**, 1757 (2000).
[57] R. Laskowski, P. Blaha, and K. Schwarz, Phys. Rev. B **67**, 075102 (2003).
[58] *CRC Handbook of Chemistry and Physics* (CRC Press, Boca Raton, FL, 1981–82), 62nd ed.
[59] G. Artioli, M. Dapiaggi, P. Fornasini, A. Sanson, F. Rocca, and M. Merli, J. Phys. Chem. Solids (in press).